


Article

Three-Phase High Power Underwater Capacitive Wireless Power Transfer System for Autonomous Underwater Vehicles

Lei Yang ^{1,*} , Liye Tian ¹, Xinze Chen ¹, Zhixue Bu ¹, Dengrui Xing ¹, Aimin Zhang ² and Xiangqian Tong ¹¹ School of Electrical Engineering, Xi'an University of Technology, Xi'an 710048, China² School of Electronic and Information Engineering, Xi'an Jiaotong University, Xi'an 710048, China

* Correspondence: yanglei0930@xaut.edu.cn

Abstract: This paper proposes a 1000 W high-frequency three-phase power inversion underwater capacitive wireless power transfer (UCWPT) system for power delivery to autonomous underwater vehicles (AUVs). The multi-phase coupling structure is designed as a columnar configuration that conforms to the shape of AUVs. This paper innovatively presents a curved coupling coupler composed of six metal plates. This design significantly enhances the mutual capacitance of the coupling structure and the power transfer capacity of the UCWPT system. Utilizing the columnar structure, the receiver of the capacitive wireless power transfer system can be easily integrated into AUVs, reducing the installation space. Furthermore, the cylindrical dock-transmitter terminal structure of the system greatly improves the anti-misalignment capability. This addresses issues such as charging voltage and current fluctuations caused by vehicle rolling in dynamic ocean environments. Additionally, the wireless power transfer capacity is notably enhanced. An experimental platform was constructed, and tests were conducted in both air and water media. A 1000 W experimental setup was developed to validate the theoretical analysis and simulations. The experimental results align closely with the theoretical predictions. At a fixed distance of 3 cm between transmitter and receiver, peak power transfer efficiencies of 80% in air and 74% in water were achieved with stable operational performance. The cylindrical structure demonstrates robust anti-misalignment properties.



Academic Editor: Yassine Amirat

Received: 20 April 2025

Revised: 6 May 2025

Accepted: 9 May 2025

Published: 20 May 2025

Citation: Yang, L.; Tian, L.; Chen, X.; Bu, Z.; Xing, D.; Zhang, A.; Tong, X. Three-Phase High Power Underwater Capacitive Wireless Power Transfer System for Autonomous Underwater Vehicles. *J. Mar. Sci. Eng.* **2025**, *13*, 989. <https://doi.org/10.3390/jmse13050989>

Copyright: © 2025 by the authors. Licensee MDPI, Basel, Switzerland. This article is an open access article distributed under the terms and conditions of the Creative Commons Attribution (CC BY) license (<https://creativecommons.org/licenses/by/4.0/>).

Keywords: underwater capacitive wireless power transfer (UWPT) system; multi-phase coupling structure; high-frequency three-phase power inversion; autonomous underwater vehicles (AUVs)

1. Introduction

Autonomous underwater vehicles (AUVs) are equipped with advanced technologies including sensors, cameras, and navigation systems that enable them to navigate underwater, gather data, and conduct the precise mapping of the ocean floor. They are used for a variety of purposes such as deep-sea exploration, underwater archeology, environmental monitoring, and oil and gas industry inspections.

AUVs also have important commercial and military uses. They are adopted in the oil and gas industry to inspect underwater pipelines and facilities, and in military operations for tasks such as mine detection and reconnaissance. Despite their advanced capabilities, AUVs do have some limitations. They are often limited by their battery life and communication range and can only be deployed in certain underwater conditions.

Since a wireless power transfer system does not require physical connections or exposed conductors, it can potentially minimize the risk of electrical hazards for both

humans and marine life. This can be particularly important in sensitive underwater environments where the presence of cables or exposed electrical components may pose risks to marine ecosystems or divers. To solve the limitation of lithium battery range, an underwater wireless power transfer (UWPT) system has been proposed to conduct convenient underwater charging of small, submerged devices such as AUVs [1–6]. There are mainly two underwater wireless power transfer methods. One is the underwater inductive wireless power transfer (UIWPT) method, which is based on high-frequency alternating magnetic fields. The other method is the underwater capacitive wireless power transfer (UCWPT) system. The underwater inductive wireless power transfer method has been deeply studied and widely used for charging AUVs [7–11].

The capacitive wireless power transfer (CWPT) method could achieve high-power transfer efficiency. This means that more of the transmitted power can reach the underwater device without significant losses, resulting in an improved overall system performance. With a CWPT system, the underwater equipment could be freely movable within a certain range from the power source. This allows for increased flexibility in positioning and orientation, enabling underwater equipment to be deployed in various configurations and be adapted to changing environmental conditions [12–16].

The permittivity of pure water and seawater is about 81 times higher than free space. Within a seawater medium, the coupling capacitance of a CWPT system could be highly improved at the same distance between the transmitter and receiver of the CWPT system compared with the air medium. If a CWPT system could be used for AUVs or other underwater sensors, it could facilitate wireless power transfer applications for underwater equipment and provide a good performance [17–20].

An IWPT coupler comprises coils, magnetic cores, and shields, whereas a CWPT coupler only requires metal plates and insulating layers, making it more cost-effective, lighter, and more reliable. In addition, CWPT couplers create highly efficient coupling capacitance, as water has higher permittivity, making them especially promising for development underwater, particularly in freshwater environments [21]. For marine environment applications, a high eddy current loss will occur with an IWPT system. However, for a CWPT system, based on the high-frequency alternating electric fields, the eddy current loss will be avoided [22–25].

For a UCWPT system, the power transfer level is always several hundred watts. The maximum available power of a dissipative capacitive power transfer (CPT) system submerged in seawater has been studied [26,27]. The power transfer level is not high enough for quick power charging. Furthermore, the capacitive coupling structure is always built with four rectangular or square metal plates. For cylindrical AUVs, the coupling structure is not easy to install and occupies a large area of internal space within an AUV. Compared with the four-pole coupling mechanism, the six-pole structure optimizes the electric field distribution, increases the coupling capacitance, and improves the transmission power by increasing the number of poles. The multi-plate layout of a six-plate structure makes the spatial electric field distribution more uniform and has a better anti-deviation ability. In addition, the six-plate structure has a higher fault tolerance, and when one coupling plate fails, the other two phases can still maintain a higher power supply. Therefore, the six-plate structure has more advantages [28]. The different kinds of capacitive coupling structures have been proposed and verified in the underwater condition. It could act as the guidance for this paper [29–31].

For underwater capacitive wireless power transfer (UCWPT) systems, single-phase alternating current (AC) has predominantly been adopted as the power supply. This paper introduces, for the first time, a three-phase AC power supply scheme and establishes the first theoretical model for coupling capacitance analysis in three-phase capacitive wireless

power transfer (WPT) systems. The proposed system addresses three-phase imbalance issues caused by asymmetric coupling mechanisms and parameter variations in compensation components, achieving 80% transmission efficiency. These results validate the system's feasibility and provide both theoretical and practical foundations for advancing three-phase capacitive WPT technology. The transmission efficiency of underwater wireless power transfer (UWPT) is critically dependent on transfer distance. To maintain high efficiency, the system requires maintaining small transfer distances. Aligned with practical engineering constraints—where underwater robots typically operate at a 3 cm separation from receiving plates—the coupling mechanism's plate spacing is designed to 3 cm. This short distance significantly increases coupling capacitance, enabling compensation inductors to maintain low inductance values (even at a resonance frequency of 500 kHz) while reducing power losses, thereby enhancing overall system efficiency. At this 3 cm transfer distance, the system demonstrates stable operation and robust tolerance to lateral misalignment up to 6 cm.

This paper proposes a 1 kW six-plate columnar capacitive coupling UCWPT system tailored for autonomous underwater vehicles (AUVs). The columnar coupling structure allows seamless integration of the receiver into AUVs, minimizing spatial footprint. Experimental results demonstrate peak power transfer efficiencies of 80% in air and 74% in seawater at a fixed 3 cm transfer distance. The cylindrical configuration inherently mitigates dynamic misalignment caused by seawater currents, exhibiting exceptional anti-misalignment characteristics. High-power operation is enabled by a multi-phase inverter topology combined with a multi-phase coupling architecture.

The rest of this paper is organized as follows: Section 2 provides the design principle of the underwater capacitive power wireless power transfer system. The three-phase capacitive coupling structure design is presented in Section 3. Section 4 provides the simulated results and the experimental verification in air condition and water condition. The conclusions and discussions are derived in Section 5.

2. Operation Analysis for Underwater Wireless Power Conversion Transfer System

As shown in Figure 1, the transmitter coupling structure consists of three curved metal plates, each forming a 100-degree arc. Correspondingly, the receiver coupling structure incorporates three symmetrically designed 100-degree arc-shaped metal plates. As a result, the power can be wirelessly transferred through the three curved metal coupling structure. The battery of AUVs could be charged between the transmitter metal coupling structure and receiver metal coupling structure.

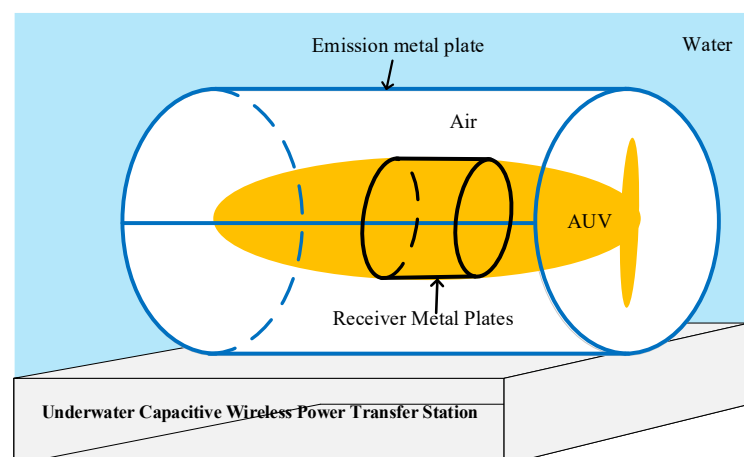


Figure 1. Three-phase UCWPT structure.

The topology of the multi-phase column underwater capacitive WPT system is shown in Figure 2. On the primary side, a three-phase inverter converts the DC voltage. An LCLC-LCLC compensation network is used to keep the system resonant. Power is transmitted via a multi-phase metallic plate capacitive coupling structure based on a high-frequency alternating electric field. On the secondary side, a full-bridge rectifier converts the high-frequency AC voltage. The output voltage and current are regulated by a controlled DC-DC converter to charge the underwater robot. Three receiver plates (with 100-degree arc) are placed inside the autonomous submersible. Three transmitter plates (100-degree arc) form a cylindrical charging dock. This enables stable wireless charging in dynamic underwater environments.

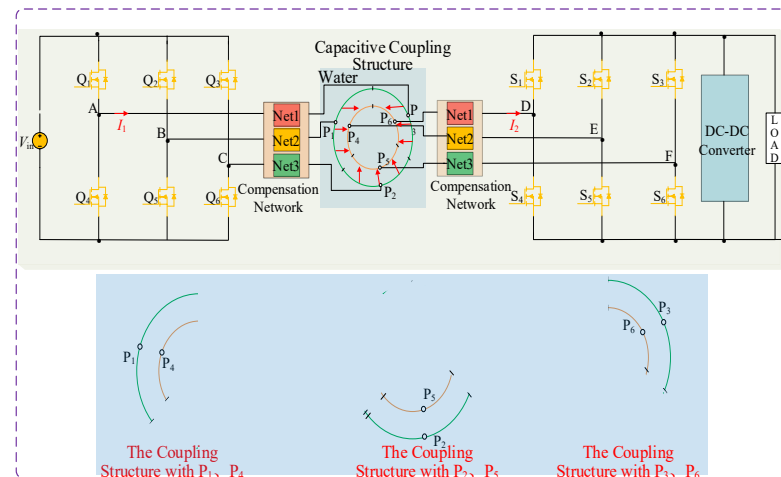


Figure 2. Topology of underwater capacitive wireless power transfer system with the three-phase column structure.

The capacitive coupling structure of the UCWPT system is shown in Figure 3. It can be seen from Figure 3 that the three-column receiving plates could build a cylindrical receiver mechanism. It will be placed inside the AUVs, which is close to the outer shell. The three-column transmitting plates could also build a larger cylindrical transmitter mechanism with a bigger diameter. As a result, the column capacitive coupling structure is constructed. It could both work in the undersea condition and the air condition. The power could be transferred through the outer shell of AUVs.

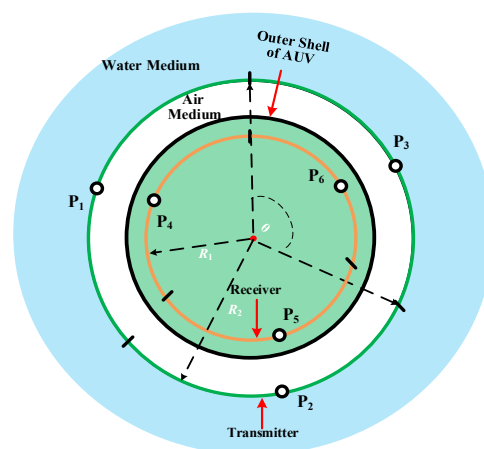


Figure 3. Cross-sectional view of three-phase coupling mechanism of underwater vehicle.

The theory analysis and the calculation are conducted in the following parts.

With the seawater medium, the dielectric constant of seawater determines the coupling capacitance. The relationship between the dielectric constant of seawater, seawater temperature, seawater salinity, and the angular frequency of electromagnetic wave is as follows:

$$\varepsilon(S, T, \omega) = \varepsilon_{\infty}(S, T) + \frac{\varepsilon_S(S, T) - \varepsilon_{\infty}(S, T)}{1 - j\omega\tau(S, T)} - j\frac{\delta(S, T)}{\omega\varepsilon_0} \quad (1)$$

where $\varepsilon_{\infty}(S, T)$ is the dielectric constant of seawater at infinite frequency, ε_0 is the dielectric constant of free space, $\omega = 2\pi f$, f is the frequency of electromagnetic wave, $\varepsilon_S(S, T)$ is the static dielectric constant of seawater, $\delta(S, T)$ is the ionic conductivity of seawater, and $\tau(S, T)$ is Debye relaxation time.

The coupling capacitance C_M of the coupling mechanism based on the arc metal plate can be expressed as follows:

$$C_M = \frac{\varepsilon_0}{\pi} \ln \frac{1 + \sin \left(\arctan \left(\frac{(a+b)^2 + c^2}{(a+b)^2 - c^2} \tan \alpha \right) \right)}{1 - \sin \left(\arctan \left(\frac{(a+b)^2 + c^2}{(a+b)^2 - c^2} \tan \alpha \right) \right)} \quad (2)$$

where ε_0 is the dielectric constant of the dielectric between plates, a , b , and c are the semi-major axis, semi-minor axis, and semi-focal length of the elliptic cylinder belonging to the curved plate, and α is the central angle of the curved metal plate.

If the curved metal plate could be transformed into a symmetrical circular column capacitor, where $a = b$ and $c = 0$, the coupling capacitor C_M can be expressed as follows:

$$C_M = \frac{\varepsilon_0}{\pi} \ln \frac{1 + \sin \alpha}{1 - \sin \alpha} \quad (3)$$

In the three-phase six-plate coupling structure, there is coupling between the two plates. Figure 4 shows all the coupling capacitors between the six plates (three coupling structure). C_{14} , C_{25} , and C_{36} are mutual capacitors for energy transfer between the primary and secondary sides, C_{12} , C_{23} , and C_{13} are the self-capacitance between the primary side three-phase plates, and C_{45} , C_{56} , and C_{46} are the self-capacitance between the secondary side three-phase plates. The remaining capacitors will also have an effect on the capacitance of each phase.

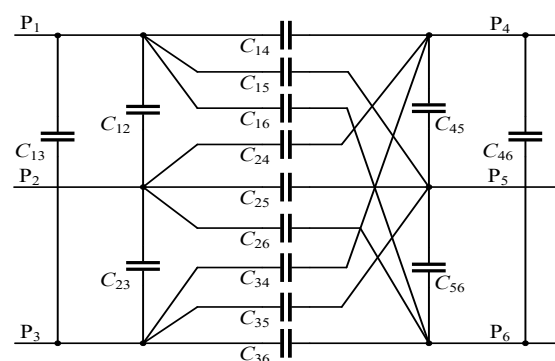


Figure 4. Full-capacitor model of a six-plate coupler.

The circuit topology and coupling mechanism of the three-phase CPT system are symmetric. As a result, the three-phase system can be simplified to a single-phase system for analysis. The simplified equivalent circuit of the single-phase coupling mechanism is shown in Figure 5a. For convenience of analysis, the circuit shown in Figure 5a is simplified into a network of the type shown in Figure 5b.

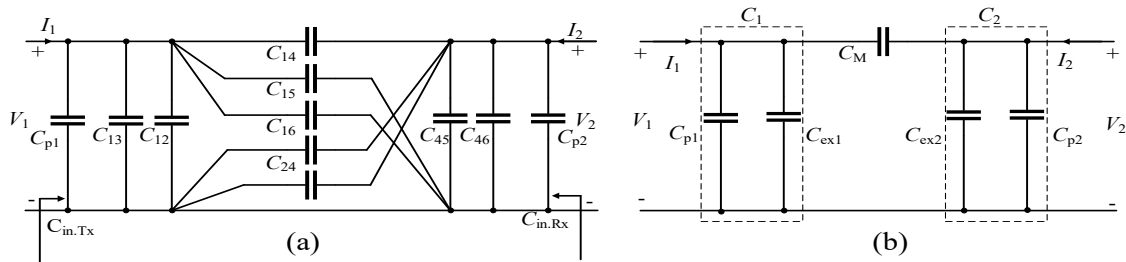


Figure 5. (a) Single-phase full capacitance equivalent circuit; (b) Simplified equivalent circuit.

3. Theory Analysis of Underwater Capacitive Wireless Power Transfer Method

As shown in Figure 5a, the A-phase input–output voltage is defined as V_1 , and V_2 . The input–output current is defined as I_1 and I_2 . The coupling mechanism is regarded as A two-port network, then the input–output relationship is shown as follows:

$$\begin{cases} I_1 = j\omega(C_{12} + C_{13} + C_{14} + C_{15} + C_{16} + C_{p1})V_1 - j\omega C_{14}V_2 \\ I_2 = -j\omega C_{14}V_1 + j\omega(C_{14} + C_{34} + C_{24} + C_{45} + C_{46} + C_{p2})V_2 \end{cases} \quad (4)$$

Similarly, the input–output relationship of the circuit model shown in Figure 5b could be expressed as follows:

$$\begin{cases} I_1 = j\omega(C_{ex1} + C_M + C_{p1})V_1 - j\omega C_M V_2 \\ I_2 = -j\omega C_M V_1 + j\omega(C_{ex2} + C_M + C_{p2})V_2 \end{cases} \quad (5)$$

The two models (Figure 5a,b) are equivalent to each other. Therefore, the equivalent parameter can be obtained by combining Equations (4) and (5):

$$\begin{cases} C_M = C_{14} \\ C_{ex1} = C_{12} + C_{13} + C_{15} + C_{16} \\ C_{ex2} = C_{34} + C_{24} + C_{45} + C_{46} \end{cases} \quad (6)$$

The C_{p1} and C_{p2} is the compensation capacitor, C_{p1} and C_{ex1} are connected in parallel, and C_{p2} and C_{ex2} are connected in parallel.

$$\begin{cases} C_1 = C_{p1} + C_{ex1} \\ C_2 = C_{p2} + C_{ex2} \end{cases} \quad (7)$$

The $C_{in.Tx}$ and $C_{in.Rx}$ is the compensation capacitor, C_{p1} and C_{p2} are connected in parallel, and C_{p1} and C_{p2} are connected in parallel,

$$\begin{cases} C_{in.Tx} = \frac{I_1}{j\omega V_1} \Big|_{I_2=0} = C_1 + C_M - \frac{C_M^2}{C_2 + C_M} \\ C_{in.Rx} = \frac{I_2}{j\omega V_2} \Big|_{I_1=0} = C_2 + C_M - \frac{C_M^2}{C_1 + C_M} \end{cases} \quad (8)$$

The Fundamental Harmonic Approximation is adopted to simplify the circuit, and the circuit is analyzed by superposition theorem. As shown in Figure 6, this approach yields a simplified circuit model for phase A of the three-phase CWPT system. The input and output voltages are represented by two AC voltage sources. The superposition theorem is used to analyze the resonant circuit separately when the input and output voltages are used as excitation.

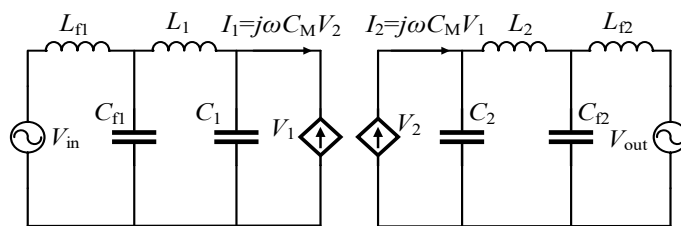


Figure 6. The simplified circuit model of phase A of the three-phase CWPT system.

Figure 7a shows that the resonant circuit is excited only by the input voltage. In this case, L_{f2} and C_{f2} form a parallel resonance, the impedance is infinite, and L_2 is regarded as an open circuit. L_1 , C_{f1} , and $C_{in.Tx}$ form another parallel resonance, and no current flows on L_{f1} . Therefore, the relationship between circuit parameters is expressed as follows:

$$\begin{cases} \omega = 2\pi f = \frac{1}{\sqrt{L_{f2}C_{f2}}} \\ L_1 = \frac{1}{\omega^2 C_{f1}} + \frac{1}{\omega^2 C_{in.Tx}} \end{cases} \quad (9)$$

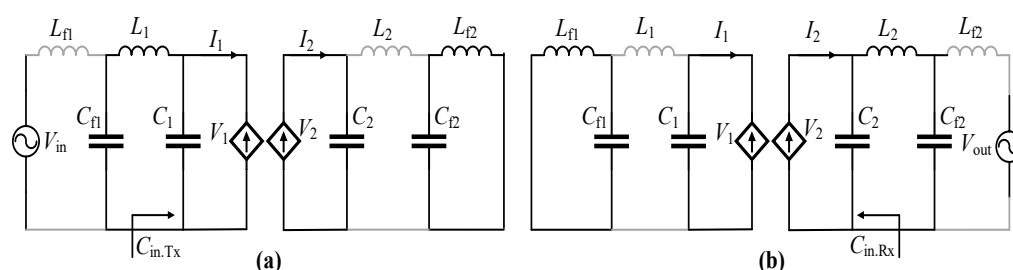


Figure 7. (a) Circuit analysis I; (b) Circuit analysis II.

Since L_{f1} and L_2 are considered as the open circuit. As a result, $V_{cf1} = V_{in}$ and $V_{cf2} = V_2$. According to Figure 7a, the following equations could be derived as follows:

$$\begin{cases} V_1 = V_{Cf1} \frac{C_{f1}}{C_{in.Tx}} = V_{in} \frac{C_{f1}}{(C_1 + C_M - \frac{C_M^2}{C_2 + C_M})} \\ V_2 = V_1 \frac{C_M}{C_2 + C_M} = V_{in} \frac{C_{f1} C_M}{C_1 C_M + C_2 C_M + C_1 C_2} \\ -I_{Lf2} = V_2 \frac{1}{j\omega L_{f2}} = V_2 \frac{\omega C_{f2}}{j} = \frac{j\omega C_{f1} C_{f2} C_M V_{in}}{(C_1 C_M + C_2 C_M + C_1 C_2)} \end{cases} \quad (10)$$

The output power could be represented as follows:

$$P_{out} = |V_{out}| |I_{Lf2}| = \frac{\omega C_{f1} C_{f2} C_M |V_{in}| |V_{out}|}{(C_1 C_M + C_2 C_M + C_1 C_2)} \quad (11)$$

Figure 7b shows that the resonant circuit is excited only by the output voltage. Where L_{f1} and C_{f1} form a parallel resonance. L_2 , C_{f2} , and $C_{in.Rx}$ form another parallel resonance. L_1 and L_{f1} are regarded as an open circuit. There are no current that flow on L_{f1} . The relationship between the related circuit parameters is expressed as follows:

$$\begin{cases} \omega = 2\pi f = \frac{1}{\sqrt{L_{f1}C_{f1}}} \\ L_2 = \frac{1}{\omega^2 C_{f2}} + \frac{1}{\omega^2 C_{in.Rx}} \end{cases} \quad (12)$$

As L_1 and L_{f2} are open circuits, $V_{cf1} = V_1$ and $V_{cf2} = V_{out}$. According to Figure 7b, the calculation of the parameters could be obtained as follows:

$$\begin{cases} V_2 = V_{Cf2} \frac{C_{f2}}{C_{in.Rx}} = V_{out} \left(\frac{C_{f2}}{C_2 + C_M - \frac{C_M^2}{C_1 + C_M}} \right) \\ V_1 = V_2 \frac{C_M}{C_1 + C_M} = V_{out} \frac{C_{f2} C_M}{C_1 C_M + C_2 C_M + C_1 C_2} \\ I_{Lf1} = V_1 \frac{1}{j\omega L_{f1}} = V_1 \frac{\omega C_{f1}}{j} = \frac{-j\omega C_{f1} C_{f2} C_M V_{out}}{(C_1 C_M + C_2 C_M + C_1 C_2)} \end{cases} \quad (13)$$

The input power could be derived as follows:

$$P_{in} = |V_{in}| \cdot |I_{Lf1}| = \frac{\omega C_{f1} C_{f2} C_M |V_{in}| |V_{out}|}{(C_1 C_M + C_2 C_M + C_1 C_2)} \quad (14)$$

As can be seen from Equations (10) and (13), the output current ($-I_{Lf2}$) is leading the input voltage, V_{in} , by 90° , and the input current is lagging the output voltage, V_{out} , by 90° . Since an uncontrolled diode rectifier is used at the secondary side, the output voltage, V_{out} , must be in phase with the output current ($-I_{Lf2}$). Therefore, the input voltage, V_{in} , is in phase with the input current, I_{Lf1} .

The phase difference, θ , between the emitter-side voltage, V_1 , and the receiver-side voltage, V_2 , of the electric field coupling mechanism can be expressed as follows:

$$\theta = \arctan\left(\frac{\omega C_{f2}^2 V_{out}^2}{C_{in.Rx} P_{out}}\right) - \arctan\left(\frac{\omega C_{f2}^2 C_M^2 V_{out}^2}{C_{in.Rx} P_{out} (C_1 + C_M)(C_2 + C_M)}\right) \quad (15)$$

4. Simulated and Experimental Verification for Underwater Capacitive Wireless Power Transfer System

The 3D model of the cylindrical coupling mechanism is shown in Figure 8. Simulation is conducted with Ansys Maxwell 16.0 software, and the parameters of column six-plate capacitive coupling structure are shown in Table 1. The switching frequency is set at 500 kHz. The simulated results are shown in Figure 9. The electric field intensity distribution is shown in Figure 9a. It can be seen from Figure 9a that the high electric field is generated. The highest electric field intensity is distributed between the transmitter plate and the receiver plate. The simulated current vector field distribution is shown in Figure 9b. As shown in Figure 9b, the current vector is distributed in the capacitive coupling structure. The power transfer capacity is verified. The column six-plate capacitive coupling structure could help to solve the charging voltage and current fluctuation caused by vehicle rolling in dynamic ocean environment.

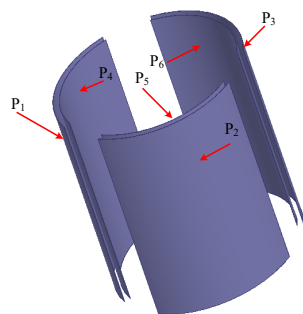


Figure 8. The 3D model of the cylindrical coupling mechanism.

Figure 10a,b illustrates the change in the coupling capacitance when the coupling plates are offset. According to the calculation formula of coupling capacitance, the coupling capacitance is related to the front of the coupling plate, and when the opposite area decreases, the coupling capacitance also decreases. As shown in Figure 10a, when the

coupling plates are rotationally offset, the facing area between them decreases, resulting in a decrease in electric field distribution between them and the coupling capacitance.

Table 1. Parameters of column Six-plate Capacitive Coupling Structure.

Elements	Parameters
Primary side plate radius R_1	150 mm
Secondary side plate radius R_2	120 mm
Plate height h	600 mm
Central angle of curved plate θ	100°

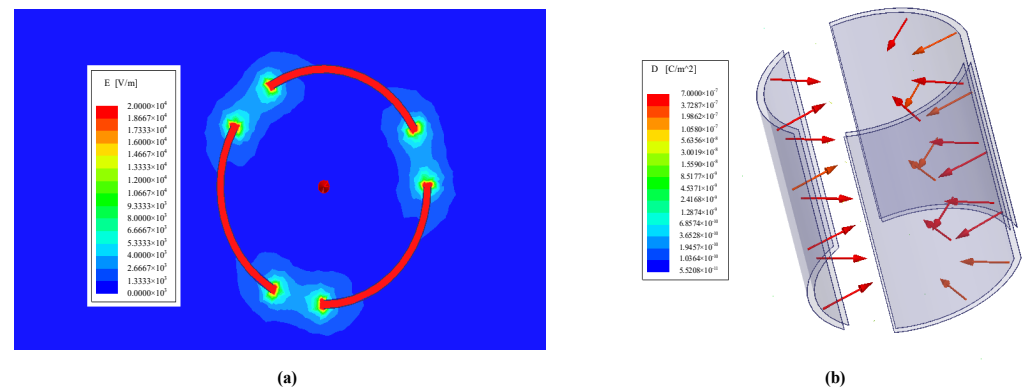


Figure 9. (a) Electric Field Intensity Distribution; (b) Current Vector Field Distribution.

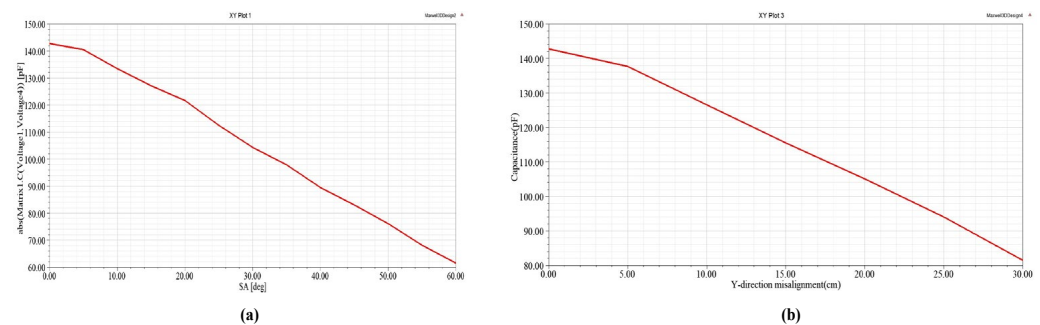


Figure 10. (a) The variation trend in coupling capacitance when the coupling plates are rotationally offset; (b) The variation trend in coupling capacitance when the coupling plates are vertically offset.

As shown in Figure 10b, when the coupling plate is vertically offset, the opposite area between them decreases, resulting in a decrease in coupling capacitance. At the same time, it can be seen that the coupling capacitance decreases more obviously when vertical offset occurs.

The UCWPT power circuit simulation is conducted with MATLAB/Simulink 2022a software. The parameters of the presented capacitive wireless power transfer system are shown in Table 2. Figure 11a shows the current waveform of each phase output by the three-phase inverter under resonant state. The three-phase phase current amplitude is equal, and the phase difference between the currents of each phase is 120 degrees. The line voltage U_{ab} , U_{bc} , and U_{ca} are all presented in Figure 11b, and the phase-shift between those voltages is also 120° .

Table 2. Parameters of Capacitive Wireless Power Transfer System.

Elements	Parameters
f	500 kHz
$C_{p1}, C_{p2}, C_{p3}, C_{p4}, C_{p5}, C_{p6}$	600 pF
$L_{f1}, L_{f2}, L_{f3}, L_{f4}, L_{f5}, L_{f6}$	28.54 μ H
$C_{f1}, C_{f2}, C_{f3}, C_{f4}, C_{f5}, C_{f6}$	3.55 nF
$L_1, L_2, L_3, L_4, L_5, L_6$	158.2 μ F

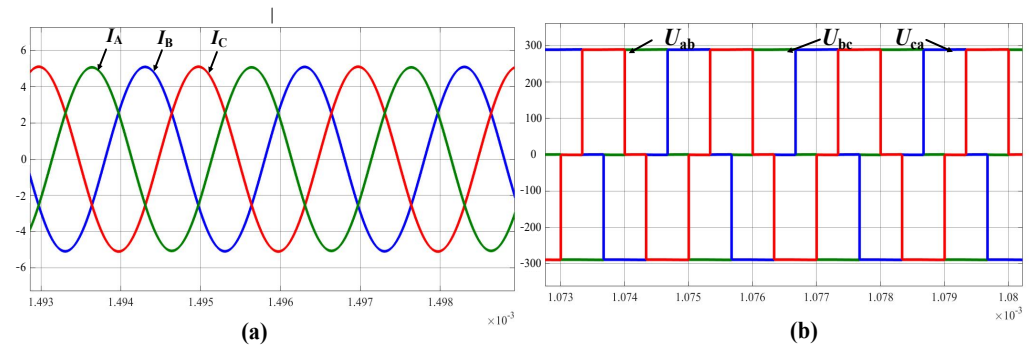
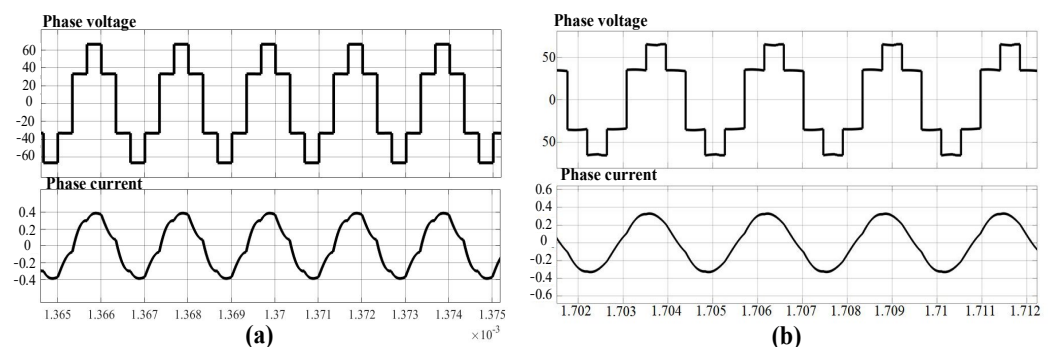
**Figure 11.** (a) Three-phase current; (b) Three-phase line voltage.

Figure 12a,b provide waveforms related to the phase current and voltage of the A-phase transmitter and receiver. As shown in the figure, the phase current, I_A , and the voltage, U_A , of the primary and secondary sides are in the same phase and can realize the zero phase angle, so that the system operates under the condition of complete resonance, thereby maximizing the active power transmission and reducing the energy loss. At the same time, we can see that the voltage gain is close to 1, which is also consistent with the realization results.

**Figure 12.** (a) Transmitting end resonance waveform; (b) Receiver resonance waveform.

The experimental setup is shown as Figure 13 with the column six-plate capacitive coupling structure. The system parameters are shown in Table 2. The experiments are conducted in the air condition. The full bridge inverter circuit and full bridge rectifier circuit are used for inverting voltage and filtering voltage, respectively. The LCLC-LCLC compensation network is adopted in this paper. The three-column receiver metal plates (120° arc) is placed in AUVs to act as the receivers. The three-column transmitter metal plates (120° arc) build a cylindrical charging dock. The battery could be wirelessly charged through the high frequency alternating electric fields when the AUVs enter and stop in the cylindrical charging dock in the water environment. With the column capacitive coupling structure, the wireless charging could be conducted in a dynamic marine environment with ocean effects.

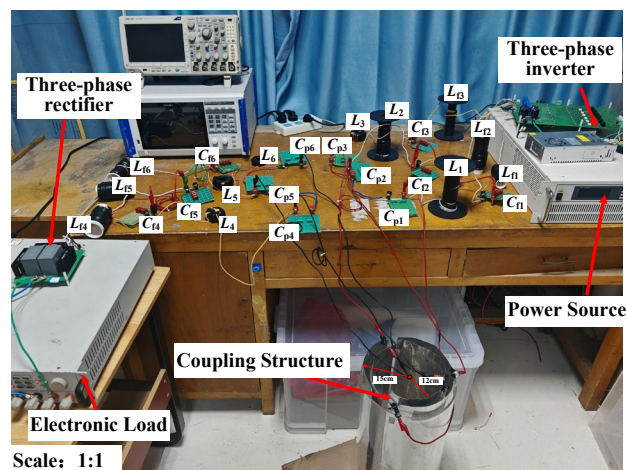


Figure 13. Experimental setup in the air condition.

The experimental results of the capacitive wireless power transmission (CWPT) system in the air medium are shown in Figure 14. Figure 14a describes the phase current waveforms output by the three-phase inverter when the system works in a resonant state. As shown in the figure, the amplitudes of the three-phase phase currents are equal, and each phase current presents a phase difference of 120° relative to other phase currents. Figure 14b shows the resonance relationship between primary and secondary phase voltages and phase currents. U_A and I_A are the primary phase voltage and phase current, and U_D and I_D are the secondary phase voltage and phase current. It can be seen that the primary and secondary phase voltages and phase currents are in the same phase, which shows that the system is in a resonant state, which is basically consistent with the simulation waveform. Figure 14c shows the three-phase line voltage, each phase has the same amplitude, and there is a 120° phase difference between them. The experimental results show that the proposed CWPT system realizes the resonance state in air medium and the maximum wireless power transmission capacity of 800 W, and the peak efficiency is 80%.

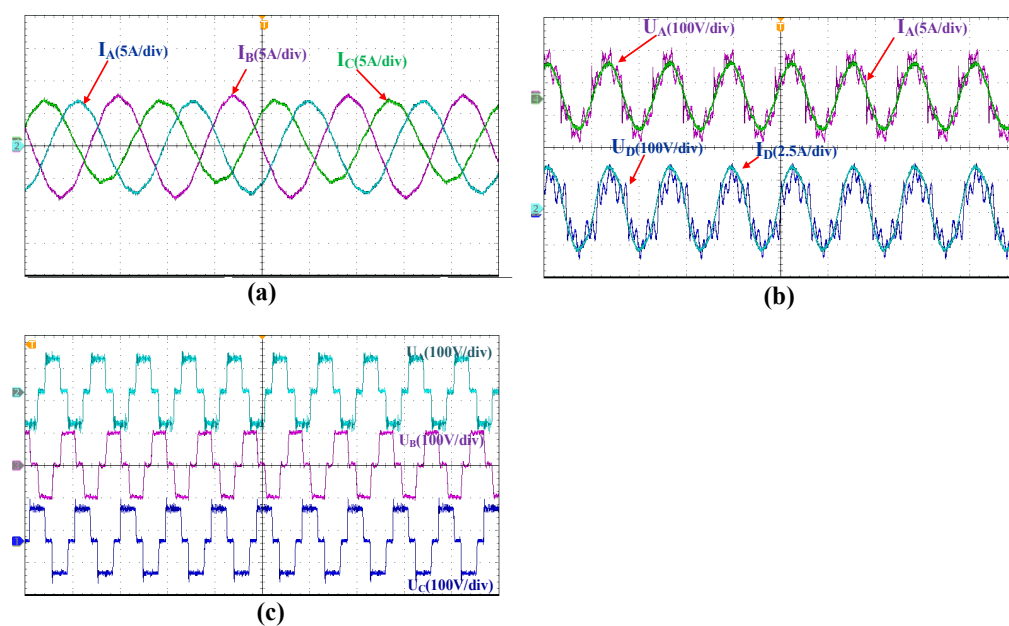


Figure 14. (a) Three-phase current; (b) Resonance waveform of transmitter and receiver; (c) Three-phase line voltage.

The power analyzer is manufactured by HIOKI Company in Shanghai, China. The Mixed Domain Oscilloscope is produced by Tektronix Company in Shanghai, China. The load is produced by ITECH Company in Nanjing, China. The inverter, rectifier, coupling mechanism and compensation network are produced by the author team.

Figure 15 shows that the power efficiency of the system is 80% at 800 W underwater, and the transmission efficiency is 76% when it is close to 600 W.

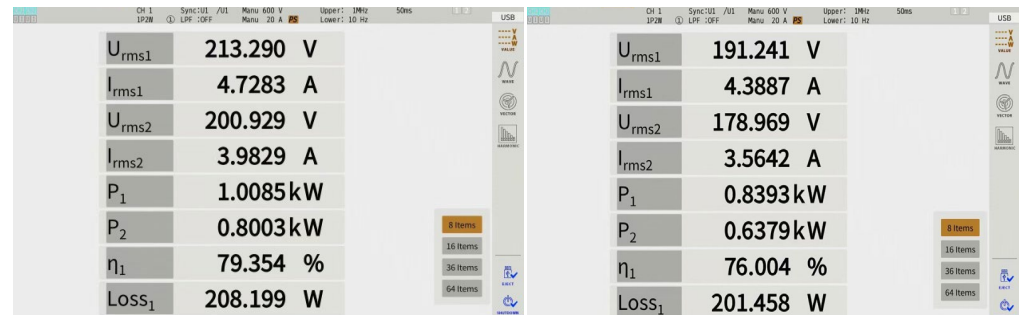


Figure 15. Experimental data of the UCWPT system in air medium.

As shown in Figure 16, the relationship between the distance between the coupling plates and the transmission efficiency shows that with the increase in the transmission distance, the transmission efficiency begins to decline slowly and then drops sharply.

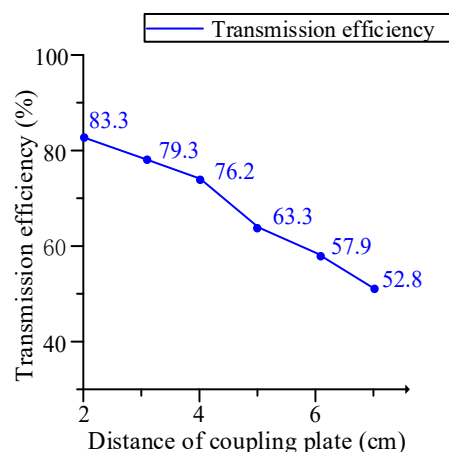


Figure 16. Relationship between distance of coupling plates and transmission efficiency.

When the vehicle enters the cylindrical charging pile, close the entrance, drain the water, and charge. The underwater test platform is shown in Figure 17. The conductivity of seawater is 5.3 S/m, and the dielectric constant is 73.

The coupling mechanism is placed in seawater, and the experimental results are shown in Figure 18. Figure 18a describes the phase current waveform output by the three-phase inverter when the system works in a resonant state. As shown in the figure, the amplitudes of the three-phase phase currents are slightly different, and each phase current has a phase difference of 120 relative to other phase currents. Figure 18b shows the resonant relationship between primary and secondary phase voltages and phase currents. Consistent with the experimental waveform in air, U_A and I_A are the primary phase voltage and phase current, and U_D and I_D are the secondary phase voltage and phase current. The primary and secondary phase voltages and phase currents are in phase, indicating that the system is in a resonant state. Therefore, the UCWPT system can operate normally in an underwater environment.

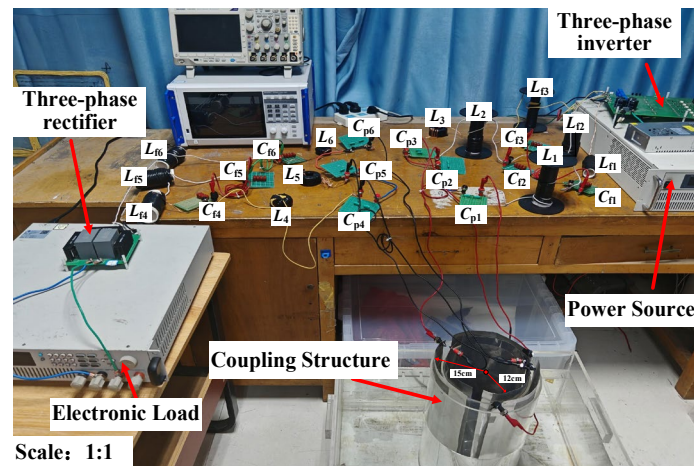


Figure 17. Experimental setup underwater.

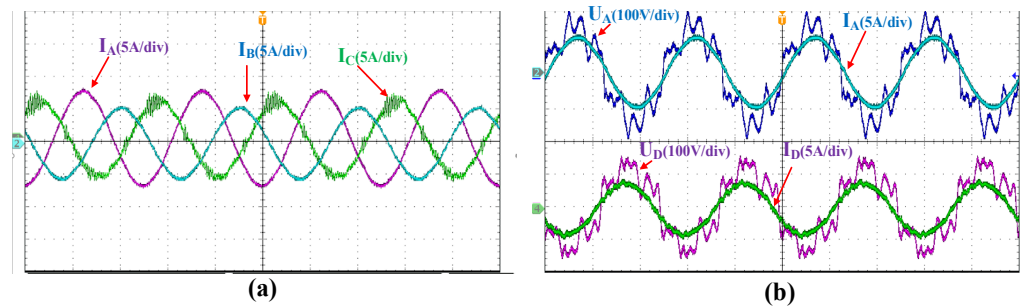


Figure 18. (a) Waveform of three-phase phase current in seawater medium; (b) Resonance waveform of transmit and receiver in seawater medium.

The barrel coupling structure has good anti-migration. The resonance waveforms of the system at different offset distances are shown in Figure 19.

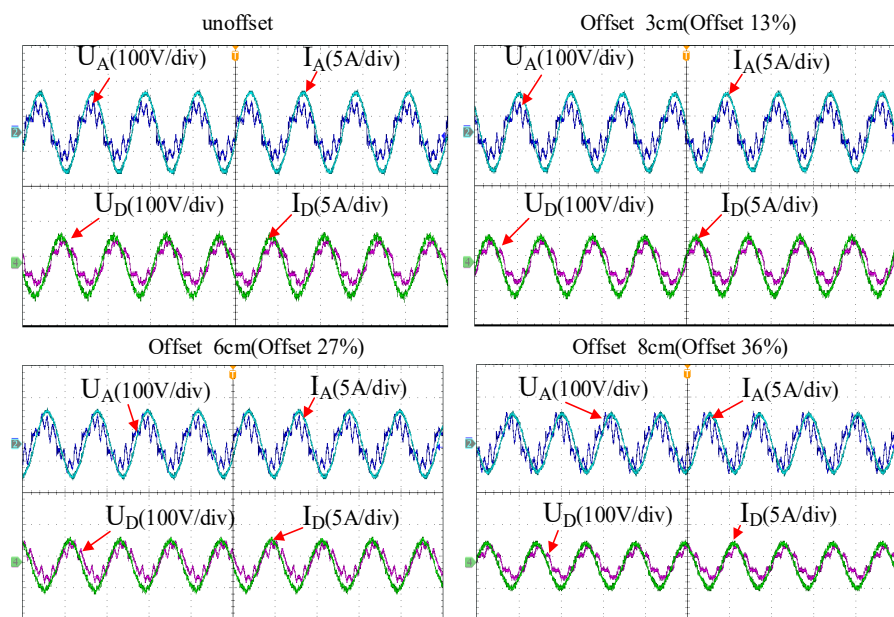


Figure 19. The UCWPT system anti-offset verification.

The single arc length of the coupling mechanism is 22 cm. As shown in Figure 18, when the deviation is 3 cm, there is no obvious change. When the deviation is 6 cm, the voltage and current at the transmitter are slightly different; when the deviation is 8 cm,

there is an obvious phase deviation between current and voltage. The results show that the coupling mechanism has good anti-drift performance.

The experimental data of the UCWPT system in seawater medium are shown in Figure 20. The power efficiency of the system is 74% at 500 W underwater, and the transmission efficiency is 72% when it is close to 1000 W.

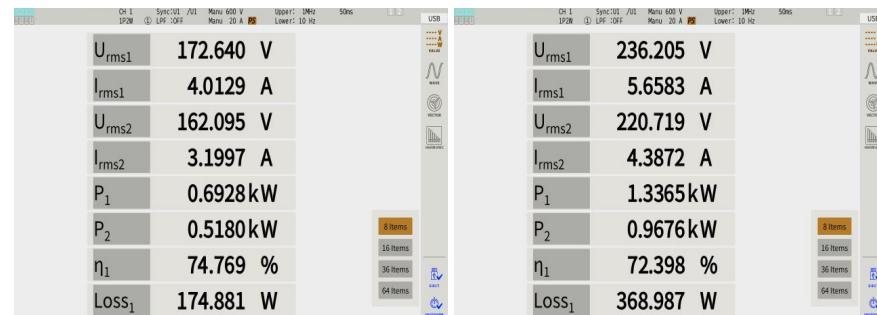


Figure 20. Experimental data of the UCWPT system in seawater medium.

The maximum power in the air of wireless power transmission system is 800 W, and the maximum efficiency is 80%. The maximum power in seawater environment is 1000 W, and the maximum efficiency is 74%. When the load is set to 50 Ω , the peak efficiency of 80% can be achieved. The results show that the experimental results are in good agreement with the theoretical analysis, and simulation results of good performance verify the superiority of the system.

5. Conclusions and Discussions

This paper proposes a column multi-phase coupling structure based underwater capacitive wireless power transfer system for AUVs. The power transfer capacity is improved with the multi-phase power inversion topology. The anti-misalignment is also highly promoted with the column structure with the easy installation in the AUVs. The battery of AUVs could be charged with any angle between the transmitter metal coupling structure and receiver metal coupling structure. This wireless power transfer method is not sensitive to the metallic foreign body and the underwater electromagnetic environment. The underwater eddy current loss could be sharply reduced based on the high frequency alternating electronic fields. A 1000 W power level experimental prototype is built for theory analysis and functions verification. When operating stably at rated power, the maximum energy transfer efficiency is up to 80% in the air medium and up to 74.7% in the water medium. The power transfer distance is 3 cm with a strong anti-misalignment ability. It meets the 360-degree rotary charging requirements. The experimental results have a good match with the simulated results and the theory analysis presented in this paper. This paper will help to accelerate practical applications of UCWPT systems for underwater mobile equipment.

Author Contributions: Conceptualization, writing—original draft preparation, L.Y. and L.T.; methodology, writing—review and editing, L.Y., L.T., X.C. and Z.B.; software, L.T. and X.T.; validation, data curation, L.Y., L.T., X.C., Z.B., D.X. and A.Z.; formal analysis, L.Y. and L.T.; investigation, D.X. and Z.B.; resources, L.Y. and X.T.; visualization, L.Y. and X.T.; supervision, L.Y. and A.Z.; project administration, funding acquisition, L.Y. All authors have read and agreed to the published version of the manuscript.

Funding: This work was supported by the National Natural Science Foundation of China under grant no. U2106218, the National Natural Science Foundation of China under grant no. 52267019, the National Natural Science Foundation of China under grant no. 52107205, the Foundation of The International Science and Technology Cooperation Center of Renewable Energy and Hybrid Power, Shaanxi, the China Postdoctoral Science Foundation under Grant no. 2023MD734218, the Key Research and Development Plan Project of Shaanxi Province under grant no. 2024GX-YBXM-255, the Qin Chuang Yuan “Scientist + Engineer” Team Building Project of Shaanxi Province under grant no. 2024QCY-KXJ-034, Xi’an Key Laboratory under grant no. 24ZDSY0015, Shaanxi Provincial Department of Education Service Local Special Project Program under grant no. 24JC067, the Natural Science Basic Research Plan in Shaanxi Province of China under Grant no. 2024JC-YBQN-0618, and the Xi’an Science and Technology Plan Project under grant no. 23GXF0069.

Data Availability Statement: The raw data supporting the conclusions of this article will be made available by the authors on request.

Conflicts of Interest: The authors declare no conflicts of interest.

References

1. Zeng, Y.; Lu, C.; Liu, R.; He, X.; Rong, C.; Liu, M. Wireless Power and Data Transfer System Using Multidirectional Magnetic Coupler for Swarm AUVs. *IEEE Trans. Power Electron.* **2022**, *38*, 1440–1444. [\[CrossRef\]](#)
2. Yan, Z.; Wu, M.; Zhao, C.; Hu, Q.; Zhu, L.; Qiao, L.; Wang, L. Free-Rotation Wireless Power Transfer System Based on Composite Anti-Misalignment Method for AUVs. *IEEE Trans. Power Electron.* **2023**, *38*, 4262–4266. [\[CrossRef\]](#)
3. Cai, C.; Li, J.; Wu, S.; Qin, Z.; Chai, W.; Yang, S. A Bipolar and Unipolar Magnetic Channel Multiplexed WPT System with Simultaneous Full-Duplex Communication for Autonomous Underwater Vehicles. *IEEE Trans. Power Electron.* **2023**, *38*, 15086–15090. [\[CrossRef\]](#)
4. Wang, D.; Chen, F.; Zhang, J.; Cui, S.; Bie, Z.; Zhu, C. A Novel Pendulum-Type Magnetic Coupler with High Misalignment Tolerance for AUV Underwater Wireless Power Transfer Systems. *IEEE Trans. Power Electron.* **2023**, *38*, 14861–14871. [\[CrossRef\]](#)
5. Wang, Y.; Li, T.; Zeng, M.; Mai, J.; Gu, P.; Xu, D. An Underwater Simultaneous Wireless Power and Data Transfer System for AUV with High-Rate Full-Duplex Communication. *IEEE Trans. Power Electron.* **2022**, *38*, 619–633. [\[CrossRef\]](#)
6. Mostafa, A.; Wang, Y.; Tangirala, S.; Zhang, H.; Lu, F. A 5 kW Hull-Compatible Inductive Charging System with 360° Folded Spatial Unipolar Coupler for Autonomous Underwater Vehicles (AUVs). *IEEE Trans. Ind. Appl.* **2023**, *59*, 7001–7012. [\[CrossRef\]](#)
7. Zhang, K.; Dai, F.; Li, X.; Yan, Z.; Zhang, F.; Mao, Z.; Hu, A.P. Analysis of Power Transfer Characteristics of IPT System with Near Field Magnetic Coupling. *IEEE Trans. Electromagn. Compat.* **2023**, *65*, 890–899. [\[CrossRef\]](#)
8. Wang, Y.; Mostafa, A.; Zheng, Z.; Zhang, H.; Zhu, C.; Lu, F. Experimental Investigation of the Eddy-Current and Dielectric Loss of Underwater IPT System. In Proceedings of the 2023 IEEE Energy Conversion Congress and Exposition (ECCE), Nashville, TN, USA, 30 October–3 November 2023; pp. 6371–6375.
9. Wu, S.; Cai, C.; Wang, A.; Qin, Z.; Yang, S. Design and Implementation of a Uniform Power and Stable Efficiency Wireless Charging System for Autonomous Underwater Vehicles. *IEEE Trans. Ind. Electron.* **2022**, *70*, 5674–5684. [\[CrossRef\]](#)
10. Zhang, B.; Chen, J.; Wang, X.; Xu, W.; Lu, C.; Lu, Y. High-Power-Density Wireless Power Transfer System for Autonomous Underwater Vehicle Based on a Variable Ring-Shaped Magnetic Coupler. *IEEE Trans. Transp. Electr.* **2023**, *10*, 3061–3074. [\[CrossRef\]](#)
11. Li, Y.; Xie, K.; Ying, Y. A Novel Magnetic Coupler with Low Leakage EMF for AUV Wireless Power Transfer System. *IEEE J. Emerg. Sel. Top. Ind. Electron.* **2023**, *5*, 212–224. [\[CrossRef\]](#)
12. Keshavarz, R.; Majidi, E.; Raza, A.; Shariati, N. Ultra-Fast and Efficient Design Method Using Deep Learning for Capacitive Coupling WPT System. *IEEE Trans. Power Electron.* **2023**, *39*, 1738–1748. [\[CrossRef\]](#)
13. Gu, W.; Qiu, D.; Shu, X.; Zhang, B.; Xiao, W.; Chen, Y. A Constant Output Capacitive Wireless Power Transfer System Based on Parity-Time Symmetric. *IEEE Trans. Circuits Syst. II Express Briefs* **2023**, *70*, 2585–2589. [\[CrossRef\]](#)
14. Rashid, S.S.; Etta, D.; Maji, S.; Afridi, K.K. Design of a High-Power Density Multi-MHz Capacitive Wireless Power Transfer System for Mobile Robots. In Proceedings of the 2023 IEEE Energy Conversion Congress and Exposition (ECCE), Nashville, TN, USA, 30 October–3 November 2023; pp. 1640–1645.
15. Savio, S.; Gillani, S.M.H.; Pratik, U.; Chattopadhyay, R.; Husain, I.; Pantic, Z. An Integrated Capacitive Power Transfer System for Field Excitation of Wound Field Synchronous Machine. In Proceedings of the 2023 IEEE Applied Power Electronics Conference and Exposition (APEC), Orlando, FL, USA, 19–23 March 2023; pp. 829–835.
16. Jiang, C.; Wei, B.; Xu, C.; Wu, X.; He, H. Efficiency Improvement Under Coupler Misalignment for Dual-Transmitter and Single-Receiver Capacitive Power Transfer System. *IEEE Trans. Power Electron.* **2023**, *38*, 14872–14883. [\[CrossRef\]](#)

17. Yang, L.; Chen, X.; Miao, S.; Zhang, Y.; Feng, B.; Cheng, Z.; Zhang, A.; Yang, T. Coupling Capacitor Structure Model of Underwater Capacitive Wireless Power Transfer System. In Proceedings of the 2023 IEEE 14th International Symposium on Power Electronics for Distributed Generation Systems (PEDG), Shanghai, China, 9–12 June 2023; pp. 94–98.
18. Rong, E.; Sun, P.; Zhang, X.; Yang, G.; Wu, X. 3.3 kW Underwater Capacitive Power Transfer System for Electric Ship Charging Application. In Proceedings of the 2023 IEEE International Conference on Power Science and Technology (ICPST), Kunming, China, 5–7 May 2023; pp. 1052–1057.
19. Yang, L.; Zhang, Y.; Li, X.; Jian, J.; Wang, Z.; Huang, J.; Ma, L.; Tong, X. Analysis and design of four-plate capacitive wireless power transfer system for undersea applications. *CES Trans. Electr. Mach. Syst.* **2021**, *5*, 202–211. [[CrossRef](#)]
20. Sun, Z.; Wang, Y.; Li, T.; Mai, J.; Zeng, M.; Xu, D. Performance Assessment of Capacitive Power Transfer in Water with Varied Conductivity. In Proceedings of the 2023 IEEE 3rd International Conference on Industrial Electronics for Sustainable Energy Systems (IESES), Shanghai, China, 26–28 July 2023; pp. 1–4.
21. Rong, E.; Sun, P.; Qiao, K.; Zhang, X.; Yang, G.; Wu, X. Six-Plate and Hybrid-Dielectric Capacitive Coupler for Underwater Wireless Power Transfer. *IEEE Trans. Power Electron.* **2023**, *39*, 2867–2881. [[CrossRef](#)]
22. Kodeeswaran, S.; Gayathri, M.N.; Kannabhiran, A.; Williamson, S.S. Design of a Static Capacitive Power Transfer System with Six-Plate Coupler for Electric Vehicle Wireless Charging. *IEEE Trans. Transp. Electr.* **2023**, *10*, 3927–3939. [[CrossRef](#)]
23. Liu, W.; Luo, B.; He, X.; Wang, Z.; Mai, R. Analysis of compensation topology with constant-voltage/current output for multiple loads capacitive power transfer system. *CSEE J. Power Energy Syst.* **2025**, *11*, 802–814. [[CrossRef](#)]
24. Basak, S.; Kundu, U.; Umanand, L. A Systematic Approach for Characterization of Capacitive Couplers for Wireless EV Charging. *IEEE Trans. Ind. Electron.* **2023**, *71*, 10422–10432. [[CrossRef](#)]
25. Mostafa, T.M.; Khater, M.; Ahmed, S. Adaptive Capacitive Power Transfer System utilizing Switch-Controlled Capacitor and DC-DC Converter. In Proceedings of the 2023 IEEE Wireless Power Technology Conference and Expo (WPTCE), San Diego, CA, USA, 4–8 June 2023; pp. 1–5.
26. Mahdi, H.; Hoff, B.; Østrem, T. Maximum Available Power of Undersea Capacitive Coupling in a Wireless Power Transfer System. In Proceedings of the 2021 IEEE Wireless Power Transfer Conference (WPTC), San Diego, CA, USA, 1–4 June 2021; pp. 1–4.
27. Zhang, H.; Lu, F. Feasibility Study of the High-Power Underwater Capacitive Wireless Power Transfer for the Electric Ship Charging Application. In Proceedings of the 2019 IEEE Electric Ship Technologies Symposium (ESTS), Washington, DC, USA, 14–16 August 2019; pp. 231–235.
28. Wang, Z.; Zhang, Y.; He, X.; Luo, B.; Mai, R. Research and Application of Capacitive Power Transfer System: A Review. *Electronics* **2022**, *11*, 1158. [[CrossRef](#)]
29. Yang, L.; Ma, L.; Huang, J.; Fu, Y. Characteristics of Undersea Capacitive Wireless Power Transfer System. In Proceedings of the 2020 IEEE 9th International Power Electronics and Motion Control Conference (IPEMC2020-ECCE Asia), Nanjing, China, 29 November–2 December 2020; pp. 2952–2955.
30. Mahdi, H.; Hattori, R.; Hoff, B.; Under, T.Ø. Seawater Capacitive Power Transfer for Maritime Charging Applications. In Proceedings of the 2023 6th International Conference on Electrical Engineering and Green Energy (CEEGE), Grimstad, Norway, 6–9 June 2023; pp. 40–45.
31. Tamura, M.; Naka, Y.; Murai, K.; Nakata, T. Design of a Capacitive Wireless Power Transfer System for Operation in Fresh Water. *IEEE Trans. Microw. Theory Tech.* **2018**, *66*, 5873–5884. [[CrossRef](#)]

Disclaimer/Publisher’s Note: The statements, opinions and data contained in all publications are solely those of the individual author(s) and contributor(s) and not of MDPI and/or the editor(s). MDPI and/or the editor(s) disclaim responsibility for any injury to people or property resulting from any ideas, methods, instructions or products referred to in the content.